

Electronic structure study and dielectric properties of amorphous ZrO₂ and HfO₂

Aditya Sharma^{1*}, Mayora Varshney¹, Sejun Kang¹, Jaeyoon Baik¹, Tae-Kyun Ha¹,
Keun-Hwa Chae², Shalendra Kumar³ and Hyun-Joon Shin¹

¹Beam Line Division, Pohang Accelerator Laboratory, POSTECH, Pohang 790-784, South Korea

²Korea Institute of Science and Technology, Seoul 136-791, South Korea

³School of Materials Science and Engineering, Changwon National University, 9 Sarim dong, Changwon 641-773, South Korea

*Corresponding author. Tel: (+82) 542791767; E-mail: adityaiuac@gmail.com (Aditya Sharma), shj001@postech.ac.kr (Hyun-Joon Shin)

Received: 03 September 2015, Revised: 22 September 2015 and Accepted: 05 December 2015

ABSTRACT

ZrO₂ and HfO₂ powder samples were prepared by using the chemical precipitation method and subsequent annealing. Crystal structure, local electronic structure and dielectric constant of amorphous and crystalline powders of ZrO₂ and HfO₂ have been examined using the synchrotron X-ray diffraction, O K-edge X-ray absorption spectroscopy, Zr 3d and Hf 4f core-level X-ray photoelectron spectroscopy and temperature dependent dielectric measurements, respectively. Amorphous ZrO₂ and HfO₂ powders exhibit a local tetragonal structure, with mixed +3 and +4 valence states of Zr and Hf ions, and demonstrated the high dielectric performance. After the heat treatment, the tetragonal phase transforms into the monoclinic phase with dominant +4 valence state of Zr and Hf ions and the larger sized ZrO₂ and HfO₂ nanoparticles exhibited low dielectric constant. The manifestation of high dielectric constants in the amorphous ZrO₂ and HfO₂ samples is because of the hopping of electrons between the Zr⁺³-Zr⁺⁴ and Hf⁺³-Hf⁺⁴ networks. Copyright © 2016 VBRI Press.

Keywords: XRD; XPS; XAS; nanoparticles.

Introduction

Zirconia (ZrO₂) and Hafnia (HfO₂) are known as 'twins' oxide materials with their outstanding electrochemical and dielectric properties [1, 2]. The 'twin' nature of these two oxides arises because of the (i) similar outer shell configuration (*d*², *s*²), (ii) quasi-identical nature of the atomic/ionic radii, and (iii) very close electronegativities (~1.3) of their metal atoms. Under the normal conditions of temperature and pressure both of the oxides exhibit monoclinic crystal structure (space group *P2₁/c*) and, practically, the same atomic density. When these components were annealed, they are known to transform first to the tetragonal phase and then cubic phase [3]. In terms of prevention of current leakage through the gate oxide layers, such as in metal-oxide-semiconductor field effect transistor (MOSFET) devices, nanocrystalline ZrO₂ and HfO₂ have shown their superiority over the commercial SiO₂ oxide layer because of their suitable band offsets, barrier heights, energy band gap and dielectric constants [2, 3]. The dielectric constant of tetragonal ZrO₂ was found to be two times larger than that of monoclinic ZrO₂ [2]. Hence, it is advantageous to achieve the tetragonal polymorphous of ZrO₂ or HfO₂ for their practical applications.

Efforts have been made to stabilize the tetragonal or cubic phase of ZrO₂ and HfO₂ at room temperature. In this context, trivalent dopants [4] and tetravalent dopants [5] have been incorporated into the host monoclinic ZrO₂. The stabilizers, nevertheless, stabilize the tetragonal or cubic phase of ZrO₂ but create oxygen vacancies and other small-sized secondary phases [6]. Such secondary phases and oxygen vacancies can degrade the structural/electrical/optical properties of the compound. Therefore alternative methods, such as 'athermal' annealing by ion-irradiation, have also been employed to stabilize the tetragonal or cubic phases of HfO₂/ZrO₂ in the thin films and powders [7, 8]. Partial phase transformation has been achieved by ion-irradiation but the high energy ion-irradiation induced defects have resulted in degradation of the crystalline quality and electrical properties of the samples. More recently, the phase stabilization by maneuvering the size of material has attracted considerable interest, introducing large surface area, extraordinary surface energy and unusual adsorptive properties of the small sized NPs [9, 10]. The surface energy of tetragonal phase is lower than that of monoclinic phase for the similar crystallite size, and the reduction of crystalline size up to a few nanometers (5-10 nm) has resulted in stabilization of the tetragonal phase of ZrO₂ at room temperature [9]. Interestingly, the amorphous gate oxides (ZrO₂ and HfO₂) are often required in the MOSFET devices because of their

isotropic and homogeneous electrical characteristics [10, 11]. In previous reports, the local monoclinic phase of ZrO_2 could be achieved in the amorphous thin films and the k value of the amorphous thin film was close to that of crystalline monoclinic structured thin film [10]. There are only few studies on the stabilization of tetragonal/cubic phase in amorphous or nanocrystalline of HfO_2 with their dielectric performance [11].

Therefore, control synthesis and atomic level understanding of the amorphous ZrO_2 and HfO_2 systems along with their dielectric performance would be valuable for the exploration of their functionalities in the futuristic devices.

Experimental

Material synthesis

Pure ZrO_2 and HfO_2 powders were synthesized using chemical precipitation method. This method has been proven its applicability to synthesize the pure and doped oxide NPs (size ~ 5 nm) [12-14]. All the reagents used were of analytical grade without further purification. To synthesize the ZrO_2 and HfO_2 powder samples, the clear solutions were prepared by dissolving the 5 gram of $\text{ZrCl}_4 \cdot 5\text{H}_2\text{O}$ and $\text{HfCl}_4 \cdot 5\text{H}_2\text{O}$ chemicals, separately, in the 200 mL double distilled (DI) water, under the constant stirring for 1 hr. When the precursor had been totally dissolved, the diluted NH_4OH solution was, drop-wise, added into the precursors. The reaction was done at 3 pH and 6 pH values of the solutions under constant stirring. The resultant precipitates were washed several times with DI water and then dried at 80 °C in air for 30 hours to obtain fine powdered samples. Further, to achieve larger grain sized HfO_2 and ZrO_2 samples, a part of the as-synthesized powders was annealed in air at 250 °C and 500 °C, respectively.

Characterization

The structural properties were examined by using the synchrotron X-ray diffraction (XRD) with $\lambda = 1.240$ Å at X-ray scattering beam line (3D beam line of Pohang Light Source (PLS), South Korea). Local electronic structure of the samples was investigated by using the near edge X-ray absorption fine structure (NEXAFS) spectroscopy at the O K-edge and the core-level X-ray photoelectron spectroscopy (XPS) at Zr 3d and Hf 4f edges. The O K-edge NEXAFS and Zr 3d and Hf 4f core-level XPS spectra were collected at the 8A beam line of the PLS. To measure the dielectric constant of the so-formed samples typical parallel plate capacitors were designed by coating the silver paste on the pellet surfaces. The dielectric response of such capacitors was measured using two electrode configuration with an Agilent 4285A precision LCR meter. These measurements were performed in the temperature range from room temperature to 500 °C, using a Lakeshore temperature controller. The real part of the complex dielectric function (k_1) was determined by considering the geometry of the parallel plate capacitor, $k_1 = Cd/(Ak_0)$, where C is the measured capacitance, d is the thickness of pellet, A is the area of pellet and k_0 is the vacuum dielectric constant.

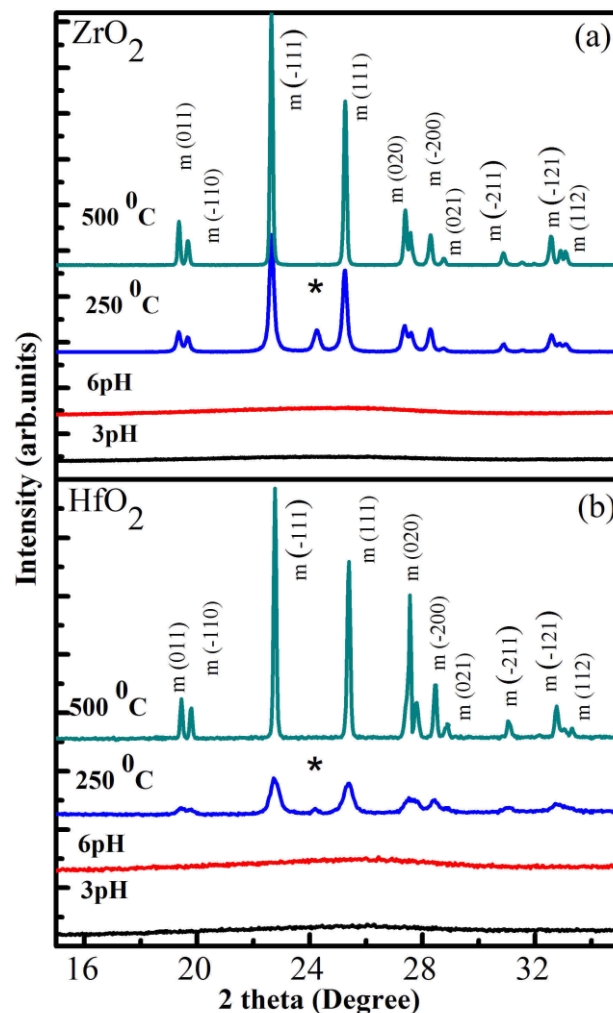


Fig. 1. (color online) XRD patterns of (a) ZrO_2 and (b) HfO_2 powders.

Results and discussion

Fig. 1(a) & (b) show the XRD patterns of ZrO_2 and HfO_2 powder samples, respectively. It is clear from the Fig. 1 that the 3 pH and 6 pH grown powders show a broad hump like feature at $\sim 25^\circ$ and do not exhibit any diffraction peak and, hence, represent the amorphous nature. The clear diffraction peaks are appeared in the XRD patterns of 250 °C and 500 °C annealed powders, indicating the polycrystalline nature of the samples. The peak identification and calculations of lattice parameters were done using the *Powder-X* software package. The XRD patterns (Fig. 1 (a)) were fairly resemble to the monoclinic ZrO_2 phase (lattice parameters; $a = 5.142$, $b = 5.20$, $c = 5.311$, angles; $\alpha = \gamma = 90^\circ$, $\beta = 99.205^\circ$, space group P21/c). Similarly the (Fig. 1 (b)) resembled to the monoclinic HfO_2 phase (lattice parameters; $a = 5.117$, $b = 5.175$, $c = 5.291$, angles; $\alpha = \gamma = 90^\circ$, $\beta = 99.216^\circ$, space group P21/c). The lattice parameters of ZrO_2 and HfO_2 powder samples closely match with the slandered JCPDF#830944 and JCPDF#780050 files, respectively. The noticeable observation in the XRD patterns of 250 °C annealed ZrO_2 and HfO_2 samples is the presence of extra peak (marked by asterisk) at $\sim 24.2^\circ$ which does not

matched with the monoclinic phase of $\text{HfO}_2/\text{ZrO}_2$. This peak resembles to the (111) peak of tetragonal phase (space group $P42/nmc$) of $\text{ZrO}_2/\text{HfO}_2$. Presence of this peak signifies the formation of mixed monoclinic and tetragonal phases in the 250 °C annealed samples. The 500 °C annealed samples show improvement in the intensity of the XRD peaks, and the (111) peak from the tetragonal phase is disappeared, indicating formation of highly crystalline monoclinic ZrO_2 and HfO_2 samples at this temperature. The average grain size (calculated by using the Scherrer relation) of 250 °C and 500 °C annealed ZrO_2 samples was ~ 15 nm and ~35 nm, respectively. For the HfO_2 samples, the size was estimated to be ~ 9 nm and ~34 nm, respectively. To further probe the morphology and particle size of the as grown and annealed samples, systematic, TEM images and selected area electron diffraction (SAED) patterns were collected.

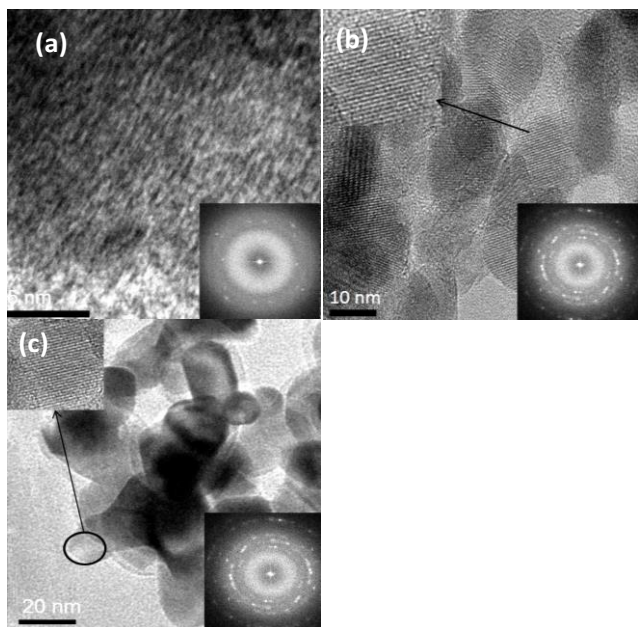


Fig. 2. (color online) TEM images of (a) 3pH grown (b) 250 °C annealed and (c) 500 °C annealed ZrO_2 powders (lower insets in TEM images show SAED patterns and upper insets show magnified view of a single particle).

Since the structural properties/phases and grain size of the ZrO_2 set of samples were very similar to that of HfO_2 set of samples, therefore, we collected the TEM and SAED investigations on the ZrO_2 set of samples only. **Fig. 2** (a), (b) and (c) present the TEM images of 3 pH grown, 250 °C annealed and 500 °C annealed ZrO_2 powders, respectively. It is clear from the **Fig. 2** (a) that 3 pH grown samples show some powder grains with no crystalline fringes and the SAED patterns also exhibited very less intense rings which are an indication of the amorphous nature of the sample. On the other hand, 250 °C annealed powder sample show (see **Fig. 2** (b)) organized particles and high intense SAED patterns, thus verify the crystalline nature. Furthermore, severe aggregation of particles can be seen in the 500 °C annealed samples (**Fig. 2** (c)). In the annealed samples, the grain growth is expected due to the sintering/ripening process of particles [15] and thus fairly polycrystalline samples are formed after the heat treatment

(evidenced by high intense SAED patterns and XRD diffraction results). The estimated particle size from the 250 °C and 500 °C annealed samples was ~ 12 nm and ~ 40 nm, respectively, and comparable with the findings of XRD data.

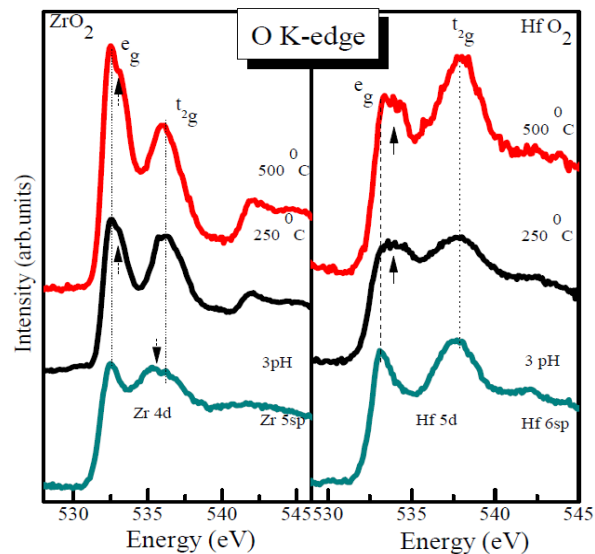


Fig. 3. (color online) O K-edge spectra of (a) ZrO_2 and (b) HfO_2 powders.

In the previous reports, it was difficult to probe the crystal structure of polymorphous samples of narrow size using the conventional techniques [9]. Local structure determination by using the synchrotron based X-ray absorption techniques is advantageous to probe the different phases of parent compound in the low dimensional NPs or even in the amorphous samples [10]. In this regard the soft X-ray NEXAFS spectra have been collected at the O K-edge from the ZrO_2 and HfO_2 powders and shall be discussed in the following sections. In the electronic structure of $\text{ZrO}_2/\text{HfO}_2$ the d bands of Zr/Hf metals are entirely empty (i.e., d^0 configuration) and O 2p bands are fully occupied. The crystal field effects, because of the electrostatic field associated with the O atoms and alignment of d orbitals with respect to O ligands, are responsible to rise the t_{2g} orbitals (group of d_{xy} , d_{xz} , and d_{yz}) and lower the e_g orbitals (group of $d_{x^2-y^2}$ and d_{z^2}) in energy [16, 17]. In case of tetragonal polymorphous the MO_8 polyhedron remains, fundamentally, cubic but there is some distortion in the crystal field [16]. Therefore, the 10 Dq values (separation of e_g and t_{2g} orbitals) will be the same to that of cubic polymorphous but some broadening or splitting of peaks (nondegeneracy in the orbitals) is expected [16-18]. On the other hand, there is no center of symmetry in the MO_7 polyhedra of monoclinic polymorphous, and therefore the individual d orbitals potentially interact with the crystal field of O atoms with unusual manner [16]. Previous reports have shown that orbital degeneracies have been removed in monoclinic ZrO_2 and there is a complex splitting of the d orbitals [19]. Moreover, it has been observed that the tetragonal polymorphous exhibits sharp e_g and splitted t_{2g} peaks and the monoclinic polymorphous exhibits splitted e_g and sharp t_{2g} peaks in the O K edge spectra [8, 10, 18]. **Fig. 3** (a) and (b) show the normalized O K-edge spectra of ZrO_2 and

HfO₂ powders, respectively. The spectral features of 3 pH grown ZrO₂ sample enclose the sharp e_g peak (~532.50 eV) and broad/split t_{2g} peak (~535.53 eV), marked by the down arrows. Similarly, the 3 pH grown HfO₂ sample also exhibit sharp e_g peak at ~533.16 eV and a broad t_{2g} peak at ~537.82 eV.

The 10 Dq value of HfO₂ (4.66 eV) is quite higher than that of ZrO₂ (3.03 eV). This is because of the fact that the 5d orbitals of Hf are more extended than the 4d orbitals of Zr. As a consequence of this, more extensive overlap with the O 2p orbitals takes place with the 5d orbitals of Hf, and thus a larger 10 Dq value is expected in case of HfO₂ [17]. The spectral features and 10 Dq values of these samples tally with those of the reported tetragonal phase of ZrO₂ and HfO₂ [10, 18-20] and therefore reinforce the view of the existence of local tetragonal structure in the amorphous ZrO₂ and HfO₂ powders. The splitting of e_g peak is seen in the 250 °C annealed powder (marked by up-arrows). These results indicate the mixture of both tetragonal and monoclinic phases in the 250 °C annealed ZrO₂/HfO₂ samples. In the XRD patterns, mixture of tetragonal and monoclinic phase was observed in the 250 °C annealed ZrO₂ and HfO₂ powders. Thus the O K-edge spectra tally our XRD data. Furthermore, the 500 °C annealed HfO₂ and ZrO₂ powders show dominant splitting in the e_g peaks and sharp t_{2g} peaks and resemble to those of bulk monoclinic local structure of ZrO₂ and HfO₂ [18-20].

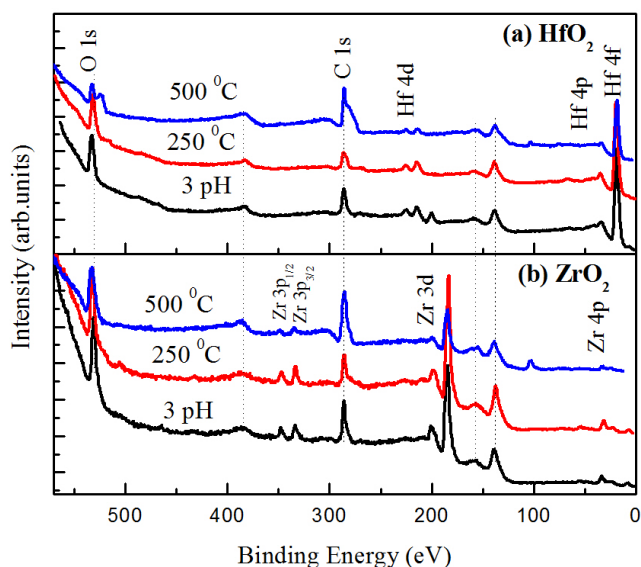


Fig. 4. (color online) XPS survey spectra of (a) HfO₂ and (b) ZrO₂ powders.

The elemental analysis of the samples was done by collecting the XPS survey spectra. **Fig. 4 (a)** and **(b)** represent the XPS survey spectra of HfO₂ and ZrO₂ samples, respectively. It is visible from the **Fig. 4 (a)** and **(b)** that the HfO₂ and ZrO₂ samples exhibit peaks mainly from the Hf and O (in HfO₂ samples) and Zr and O (in ZrO₂ samples) indicating substantial presence of the constituent elements in their parent compounds. However, peaks at 137 eV, 155.7 eV, 285.1 eV and 375 eV were present in all of the samples. The peaks at 137 eV and 155.7 eV are due to the Auger peaks of O, peak at 285.1 eV

due to the C 1s transition and the peak at 357 eV is due to the Auger transition of C.

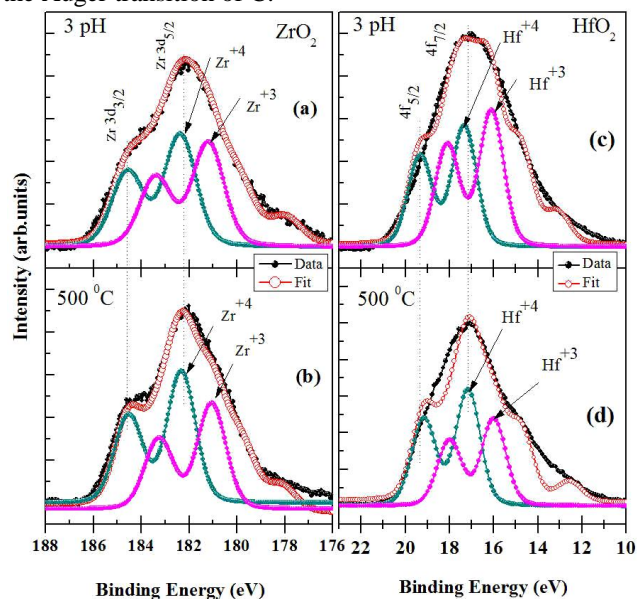


Fig. 5. (color online) Zr (3d) core-level XPS spectra of (a) 3pH grown and (b) 500 °C annealed ZrO₂ powders. Hf (4f) core-level XPS spectra of (c) 3pH grown and (d) 500 °C annealed HfO₂ powders.

To determine the valence state of Zr and Hf, systematic, Zr 3d and Hf 4f core-level XPS spectra were also collected from the 3 pH and 500 °C annealed samples. **Fig. 5 (a)** and **(b)** show the Zr 3d core-level XPS spectra of 3 pH and 500 °C annealed ZrO₂ powders, respectively. It is visible from the **Fig. 5** that Zr 3d core level spectra consist of two main peaks associated with the Zr 3d_{5/2} at binding energy 182.2 eV and 3d_{3/2} at binding energy 184.5 eV. XPS spectra were deconvoluted by using the spin-orbit splitting energy 2.3 eV and the intensity ratio of 3d_{3/2} and 3d_{5/2} peaks was 2:3. The Lorentzian and Gaussian line widths were taken to be 0.2 eV and 1.3 eV, respectively. The fitted curves suggest that the Zr exists in the mixed valence states (i.e., Zr⁺⁴ and Zr⁺³). Peaks at 181 eV and 183.3 eV contribute to the Zr⁺³ and peaks at 182.3 eV and 184.55 eV are corresponding to the Zr⁺⁴. The energy position of Zr⁺⁴ and Zr⁺³ peaks is in good agreement with the previous reports [21, 22]. Closer look of the spectra revealed that the contribution from the Zr⁺³ is comparable to that of Zr⁺⁴ in case of 3 pH grown sample; however, Zr⁺³ contribution decreased in the 500 °C annealed sample. **Fig. 5 (c)** and **(d)** show the Hf 4f core-level spectra of 3 pH grown and 500 °C annealed HfO₂ samples, respectively. Peaks at binding energy of 17.1 eV and 19.4 eV are the transitions from the Hf 4f_{7/2} and 4f_{5/2} states, respectively. Energy position of these peaks fairly resembles to those of reported HfO₂ powders [23]. Further, the deconvolution of the peaks indicates that the 3 pH grown sample contains higher Hf⁺³ component, but Hf⁺⁴ component is dominant in the 500 °C annealed sample. The small shoulders at the right-side of spectra, present in all (ZrO₂ and HfO₂) samples, may arise either from the charging artifacts in such dielectric powder samples or from the Zr/Hf-carbides (C contaminants may present in the samples during the sample preparation using the chemical synthesis and annealing). However, these

shoulders did not affect the structural and/or electronic structure investigations because the Zr 3d & Hf 4f XPS main peak positions did not change and the XRD data also unaffected by the C contaminations.

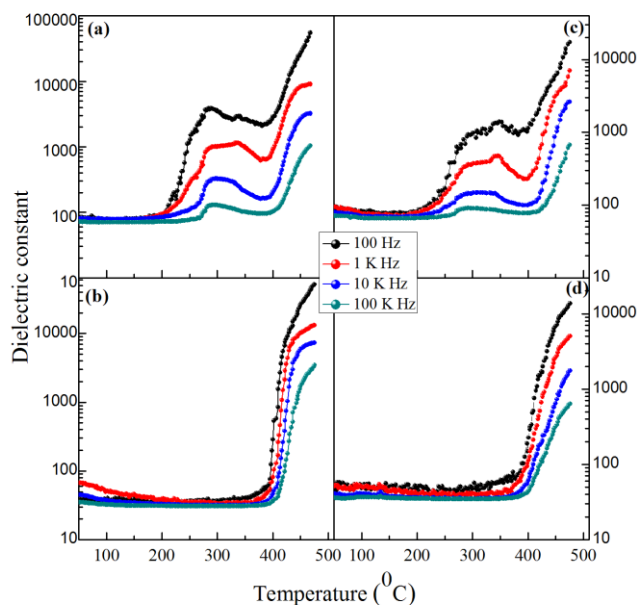


Fig. 6. (color online) Temperature dependent dielectric constant of; (a) 3pH grown ZrO_2 , (b) 500 °C annealed ZrO_2 , (c) 3pH grown HfO_2 and (d) 500 °C annealed HfO_2 powders.

To further understand the dielectric performance of the amorphous and crystalline powders, systematic, temperature dependent dielectric measurements were performed at different frequencies. **Fig. 6** shows the temperature dependency of k_f ; (a) amorphous ZrO_2 , (b) 500 °C annealed ZrO_2 , (c) amorphous HfO_2 and (d) 500 °C annealed HfO_2 , respectively. The common observation of the spectra is that the k_f decreases with increasing the operating frequency and enhances with increasing the temperature. This observation is in accordance with the Debye model. At the frequency less than $1/\tau$, where τ is the Debye relaxation time, the charge carriers contribute fully to the polarization process but the charge carriers do not follow the field reversal for the frequency larger than $1/\tau$ and thus the k_f decreases with increasing of frequency [21, 24]. Further, the k_f increases with temperature because the dipoles become free to respond with the applied field and thus favor the polarization process [24].

The most significant observation from the Fig. 6 is that the k_f is high ($\sim 10^2$ - 10^4) for the amorphous samples and decreased about an order of magnitude in the annealed samples. Furthermore, the features of dielectric spectra are quite different in amorphous and annealed samples. In the low temperature range, 50-200 °C, the k_f of amorphous ZrO_2 and HfO_2 is ~ 70 which is almost two times larger (at this temperature range) than that of annealed ZrO_2/HfO_2 and reported values [2]. In the mid temperature range, 200-375 °C, the k_f of amorphous samples show step like feature and then again increase with temperature. However, the k_f of annealed samples is ~ 22 and remains constant up to ~ 400 °C and then increase with temperature. The step like feature in the spectra of amorphous samples is ambiguous and not seen in the other reported

monoclinic/tetragonal/cubic polymorphs of ZrO_2/HfO_2 . Here, we believed that this behavior of k_f is related with the structural and electronic structure properties of the samples. XRD and O K-edge spectra exhibited the mixed tetragonal and monoclinic phases in 250 °C annealed samples which further convert into monoclinic phase at 500 °C. During the dielectric measurements of amorphous samples, as soon as the temperature rise up to 200 °C, the mixed tetragonal-monoclinic phase may form in the samples and thermally activate dipoles of mixed phases, in the presence of external field, contribute to the dielectric properties up to 375 °C. After this temperature, the dipoles of tetragonal phase get vanished and the dominating dipoles of monoclinic phase contribute to the dielectric properties of the material. The observed high k_f in the present case may be understood on the electronic structure properties of the compounds. It is known that the oxygen ions and electrons contribute to the electrical property of ZrO_2 and HfO_2 [21, 24]. It is also observed that the ionic conduction dominates in these compounds because of the small perturbation in their stoichiometry [18, 25]. Nevertheless, large surface area of small sized NPs helps to stabilize the cubic/tetragonal phase of ZrO_2/HfO_2 but also creates oxygen vacancies which indeed favor the mixed valence state of cations [21, 25].

In the present case the mixed valence state of Zr and Hf has been observed from the XPS spectra. Significant electrical conduction is expected by the hopping of electrons between Zr^{+4} - Zr^{+3} and Hf^{+4} - Hf^{+3} cation networks, as previously observed in the cubic ZrO_2 NPs [21]. Therefore, mixed valence state of cations and considerable ionic and electronic conduction seems to play a significant contribution to the observed high k_f in the amorphous/local tetragonal structured samples.

Further, our XPS results inferred that the +3 valence state of cations is significantly decreased, in the 500 °C annealed samples, which may reduce the conduction processes and thus degradation in the dielectric performance of the annealed/monoclinic structured HfO_2 and ZrO_2 samples has been observed.

Conclusion

In summary, ZrO_2 and HfO_2 powder samples were synthesized by chemical precipitation method at different pH values of solutions. Air annealing was employed to investigate the annealing induced structural, electronic structure, particle size and dielectric constant variations in the samples. It was observed that 3 pH grown amorphous ZrO_2 and HfO_2 samples have a local tetragonal structure which first converts into mixed tetragonal-monoclinic phases at low temperature (250 °C) and then transformed into dominant monoclinic phase at high temperature (500 °C). The amorphous ZrO_2 and HfO_2 samples exhibit mixed +3 and +4 valence states of Zr and Hf; however, +4 valence state of cations dominates in the annealed samples. High k_f has been observed in the amorphous samples which decreased (almost one order of magnitude) in the 500 °C annealed samples. The hopping of electrons between +3 valence state and +4 valence states of cations, which provide sufficient ionic and electrical conduction processes, are responsible for high dielectric properties of the amorphous samples.

Acknowledgements

Aditya Sharma, Mayora Varshney and Hyun-Joon Shin would like to acknowledge the financial support by the Basic Science Research Program (No. 2008-0062606, CELA-NCRC and NRF-2015R1A5A1009962) through the National Research Foundation of Korea (NRF) and by the Converging Research Centre Program (2013K000306), funded by the Korea government Ministry of Science, ICT and Future Planning (MSIP).

Author contributions

Aditya sharma and Mayora Varshney prepared the samples, collected the data and write the manuscript. Sejun Kang and Jaeyoon Baik helped in the XPS measurements and data analysis. Shalendra Kumar helped in dielectric measurements and analysis of its data. Keun-hwa Chae and Hyun-Joon Shin helped in XAS measurements, data analysis and discussions. Authors have no competing financial interests.

Reference

- G. Herrera, N. Montoya, A. Domenech-Carbo and J. Alarcon, *Phys. Chem. Chem. Phys.* **2013**, *15*, 19312.
DOI: [10.1039/C3CP53216J](https://doi.org/10.1039/C3CP53216J)
- X. Zhao and D. Vanderbilt, *Phys. Rev. B.* **2002**, *65*, 075105.
DOI: [10.1103/PhysRevB.65.233106](https://doi.org/10.1103/PhysRevB.65.233106)
- T. Yamaguchi, *Catalysis Today*, 1994, *20*, 199.
DOI: [10.1016/0920-5861\(94\)80003-0](https://doi.org/10.1016/0920-5861(94)80003-0)
- P. Li, I. W.Chen and J. E. Penner-Han, *J. Am. Ceram. Soc.* **1994**, *77*, 118.
DOI: [10.1111/j.1151-2916.1994.tb06964.x](https://doi.org/10.1111/j.1151-2916.1994.tb06964.x)
- P. Li, I. W.Chen and J. E. Penner-Han, *J. Am. Ceram. Soc.* **1994**, *77*, 1281.
DOI: [10.1111/j.1151-2916.1994.tb05403.x](https://doi.org/10.1111/j.1151-2916.1994.tb05403.x)
- S. Ostanin, A.J. Craven, D.W. McComb, D. Vlachos, A. Alavi, A. T. Paxton and M.W. Finis, *Phys. Rev. B.* **2002**, *65*, 224109.
DOI: [10.1103/PhysRevB.65.224109](https://doi.org/10.1103/PhysRevB.65.224109)
- Benyagoub, *Phys. Rev. B.* **2005**, *72*, 094114.
DOI: [10.1103/PhysRevB.72.094114](https://doi.org/10.1103/PhysRevB.72.094114)
- Sharma, M. Varshney, H. J. Shin, Y. Kumar, S. Gautam, K. H. Chae, *Chem. Phys. Lett.* **2014**, *592*, 85.
DOI: [10.1016/j.cplett.2013.12.012](https://doi.org/10.1016/j.cplett.2013.12.012)
- S. Jayakumar, P.V. Ananthapadmanabhan, T.K. Thiyagarajan, K. Perumal, S.C. Mishra, G. Suresh, L.T. Su, A.I.Y. Tok, *Mater. Chem. Phys.* **2013**, *140*, 176.
DOI: [10.1016/j.matchemphys.2013.03.018](https://doi.org/10.1016/j.matchemphys.2013.03.018)
- D. Y. Cho, H.S. Jung, J. H. Kim and C. S. Hwang, *Appl. Phys. Lett.* **2010**, *97*, 141905.
DOI: [10.1063/1.3497077](https://doi.org/10.1063/1.3497077)
- D. Ceresoilo and D. Vanderbilt, *Phys. Rev. B.*, **2006**, *74*, 125108.
DOI: [10.1103/PhysRevB.74.125108](https://doi.org/10.1103/PhysRevB.74.125108)
- Sharma, A. P. Singh, P. Thakur, N.B. Brookes, S. Kumar, C. G. Lee, R.J. Choudhary, K. D. Verma and R. Kumar, *J. Appl. Phys.*, **2010**, *107*, 093918.
DOI: [10.1063/1.3415541](https://doi.org/10.1063/1.3415541)
- Sharma, M. Varshney, H.J. Shin, Y. J. Park, M. G. Kim, T. K. Ha, K. H. Chae and S. Gautam, *Phys. Chem. Chem. Phys.*, **2014**, *16*, 19909.
DOI: [10.1039/c4cp02409e](https://doi.org/10.1039/c4cp02409e)
- Sharma, M. Varshney, Jau-hun Park, T. K. Ha, K. H. Chae, H. J. Shin, *RSC Adv.*, **2015**, *5*, 21762.
DOI: [10.1039/c4ra16217j](https://doi.org/10.1039/c4ra16217j)
- M. Petersen, A. Zangwill and C. Ratsch, *Surf. Sci.* **2003**, *536*, 55.
DOI: [10.1016/S0039-6028\(03\)00580-6](https://doi.org/10.1016/S0039-6028(03)00580-6)
- D. W. McComb, *Phys. Rev. B.* **1996**, *54*, 7094.
DOI: [10.1103/PhysRevB.54.7094](https://doi.org/10.1103/PhysRevB.54.7094)
- J. G. Chen, *Surf. Sci. Report.* 1997, *30*, 1.
DOI: [10.1016/S0167-5729\(97\)00011-3](https://doi.org/10.1016/S0167-5729(97)00011-3)
- Kikas, J. Aarik, V. Kisand, K. Kooser, T. Kaambre, H. Mandar, T. Uustare, R. Rammula, V. Sammelselg, I. Martinson, *J. Elect. Spectro. Relat. Phen.*, **2007**, *156*, 303
DOI: [10.1016/j.elspec.2006.11.031](https://doi.org/10.1016/j.elspec.2006.11.031)
- P. Crocombette and F. Jollet, *J. Phys.: Condens. Matter* **1994**, *6*, 8341.
DOI: <http://iopscience.iop.org/0953-8984/6/40/025>
- K. P. Bastos, L. Miotti, G. Lucovsky, K.B. Chung and D. Nordlund, *J. Vac. Sci. Technol. A* **2010**, *28*, 662.
DOI: [10.1116/1.3430563](https://doi.org/10.1116/1.3430563)

- S. Manna, T. Ghoshal, and S.K. De, *J. Phys. D: Appl. Phys.* **2010**, *43*, 295403.
DOI: <http://iopscience.iop.org/0022-3727/43/29/295403>
- G. M. Ingo and G. Marletta, *Nucl. Instrum. Methods. Phys. Res. B.* **1996**, *116*, 446.
DOI: [10.1016/0168-583X\(96\)00085-7](https://doi.org/10.1016/0168-583X(96)00085-7)
- D. Y. Cho, H.S. Jung and C. S. Hwang, *Phys. Rev. B.* **2010**, *82*, 094104.
DOI: [10.1103/PhysRevB.82.094104](https://doi.org/10.1103/PhysRevB.82.094104)
- K. Kumari, K. Prasad, K. L. Yadav, S. Sen, *Brazilian J. Phys.* **2009**, *39*, 279.
DOI: [10.1590/S0103-97332009000300010](https://doi.org/10.1590/S0103-97332009000300010)
- R.I. Merino and V.M. Orera, *Solid State Ion.* **1995**, *97*, 76.
DOI: [10.1016/0167-2738\(94\)00240-S](https://doi.org/10.1016/0167-2738(94)00240-S)

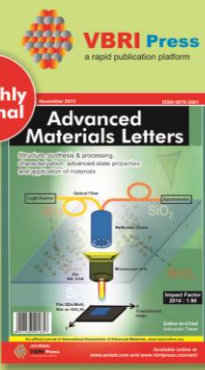
Advanced Materials Letters

Copyright © 2016 VBRI Press AB, Sweden
www.vbripress.com/aml and www.amlett.com

Publish your article in this journal

Advanced Materials Letters is an official international journal of International Association of Advanced Materials (IAAM, www.iaamonline.org) published monthly by VBRI Press AB from Sweden. The journal is intended to provide high-quality peer-review articles in the fascinating field of materials science and technology particularly in the area of structure, synthesis and processing, characterisation, advanced-state properties and applications of materials. All published articles are indexed in various databases and are available download for free. The manuscript management system is completely electronic and has fast and fair peer-review process. The journal includes review article, research article, notes, letter to editor and short communications.

A Monthly Journal



VBRI Press
a rapid publication platform

Advanced Materials Letters
Structure, synthesis and processing
Characterisation, advanced state properties
and applications of materials

Indexed Elsevier
2014 - 148